

Evolution of violent gravitational disc instability in galaxies: Late stabilization by transition from gas to stellar dominance

Marcello Cacciato^{1*}, Avishai Dekel¹ & Shy Genel^{2,3}

¹*Racah Institute of Physics, The Hebrew University, Jerusalem 91904, Israel*

²*Max-Planck-Institut für extraterrestrische Physik, Giessenbachstrasse, D-85748 Garching, Germany*

³*School of Physics and Astronomy, Tel Aviv University, Tel Aviv 69978, Israel*

ABSTRACT

We address the cosmological evolution of violent gravitational instability in high-redshift, massive, star-forming galactic discs. To this aim, we integrate in time the equations of mass and energy conservation under self-regulated instability of a two-component disc of gas and stars. The disc is assumed to be continuously fed by cold gas at the average cosmological rate. The gas forms stars and is partly driven away by stellar feedback. The gas and stars flow inward through the disc to a central bulge due to torques that drive angular momentum outwards. The gravitational energy released by the mass inflow down the gravitational potential gradient drives the disc turbulence that maintains the disc unstable with a Toomre instability parameter $Q \sim 1$, compensating for the dissipative losses of the gas turbulence and raising the stellar velocity dispersion. We follow the velocity dispersion of stars and gas as they heat and cool respectively and search for disc “stabilization”, to be marked by a low gas velocity dispersion comparable to the speed of sound $\sim 10 \text{ km s}^{-1}$. We vary the model parameters that characterize the accreted gas fraction, turbulence dissipation rate, star-formation rate, and stellar feedback. We find that as long as the gas input roughly follows the average cosmological rate, the disc instability is a robust phenomenon at high redshift till $z \sim 1$, driven by the high surface density and high gas fraction due to the intense cosmological accretion. For a broad range of model parameter values, the discs tend to “stabilize” at $z \sim 0 - 0.5$ as they become dominated by hot stars. When the model parameters are pushed to extreme values, the discs may stabilize as early as $z \sim 2$, with the gas loss by strong outflows serving as the dominant stabilizing factor.

Key words: galaxies: evolution – galaxies: formation – galaxies: haloes – galaxies: spiral – galaxies: star formation – methods: analytical

1 INTRODUCTION

According to our current understanding, high-redshift massive galaxies form in virialized dark-matter haloes that reside at the nodes of the cosmic web. When baryons are accreted into a halo along the filaments of this web (Dekel et al. 2009), angular-momentum conservation implies that most of the baryons settle into a disc, rotating with a circular velocity that is roughly comparable to the virial velocity of the halo (Fall & Efstathiou 1980; Mo et al. 1998; Bullock et al 2001; but see Danovich et al. 2011). If the disc is gravitationally unstable, with a Toomre parameter $Q \sim 1$ (Toomre 1964, see below), the velocity dispersion σ can be estimated from the circular velocity and the mass fraction in the cold disc component (e.g. Dekel, Sari & Ceverino 2009).

Pioneering observations of massive galaxies at $z \sim 2$ have

revealed striking differences between local and high-redshift star-forming discs of comparable masses and sizes (Elmegreen & Elmegreen 2005; Genzel et al. 2008). In particular, the high-redshift discs of $\sim 10^{11} M_{\odot}$ extending to $\sim 10 \text{ kpc}$ are thick, perturbed and highly turbulent, with $\sigma \sim 30 - 80 \text{ km s}^{-1}$, compared to the thin, more uniform local discs with $\sigma \sim 10 \text{ km s}^{-1}$. The high-redshift discs are gravitationally unstable, showing large transient perturbations and bound clumps of $\sim 10^9 M_{\odot}$ and sizes $\sim 1 \text{ kpc}$, as opposed to the more uniform mass distribution in typical local discs, in which the molecular clouds are smaller by a few orders of magnitude. While all discs may be gravitationally unstable to some degree, the instability in the high-redshift discs is characterized by higher velocity dispersion and more massive perturbations and thus by a more rapid dynamical evolution, such as inward migration on an orbital timescale, which we term “violent gravitational disc instability”. This is as opposed to the secular evolution associated with spiral arms and bars in low-redshift discs.

The violent instability of high redshift discs can be explained

* Minerva Fellow

E-mail: cacciato@phys.huji.ac.il

in the framework of a steady intense gas supply from the cosmic web and a rapid mass migration due to gravitational instability in the disc. The gravitational fragmentation of gas-rich, thick, turbulent discs into clumps and the subsequent migration into a central bulge have been proposed (van den Bergh et al. 1996; Elmegreen & Elmegreen 2005; Genzel et al. 2008; Bournaud et al. 2008) and successfully simulated for idealized discs in isolation (Noguchi 1999; Immeli et al. 2004; Bournaud et al. 2007). Violent gravitational disc instability in the full cosmological context has been simulated by Agertz et al. (2008) and Ceverino, Dekel & Bournaud (2010), demonstrating self-regulated instability in steady state for several Gyr. Dekel, Sari & Ceverino (2009, hereafter DSC09) applied a Toomre instability analysis (Toomre 1964) to high-redshift discs under the assumption that they are made of one cold component and fed at the average cosmological accretion rate. This analysis led to the tentative conclusion that an unstable disc at high redshift remains unstable in a cosmological steady state. This fails to account for the evolution from violently unstable discs at high redshift to marginally unstable or stable discs at low redshift, as indicated by observations and numerical simulations (e.g. § 9 in Ceverino et al. 2011; Martig et al. 2009).

In this paper, we generalize the DSC09 analysis by allowing the gas to continuously form stars. We apply a two-component disc instability analysis (Jog & Solomon 1984; Rafikov 2001; Wang & Silk 1994; Romeo & Wiegert 2011). The disc is assumed to be fed by fresh gas at a constant fraction of the average cosmological accretion rate and the gravitational instability in the disc induces mass inflow to a central bulge. The gravitational energy released by this inflow is assumed to drive velocity dispersion in the two components of the disc. With time, the dissipationless stellar component acquires high velocity dispersion, whereas the gas turbulence dissipates its energy on a dynamical timescale. We solve for the velocity dispersions of the two components under conservation of mass and energy and the assumption that the disc instability is self-regulated at a $Q \sim 1$ state. At late times, as the accretion rate decreases and the disc becomes dominated by the hot stellar component, the gas is required to have a lower velocity dispersion in order to maintain the instability. When the required gas velocity dispersion becomes comparable to the thermal speed of sound, $c_s \sim 10 \text{ km s}^{-1}$, the pressure cannot keep decreasing to the level where gravitational instability is possible, and we associate it with the end of the instability phase. We examine whether the dominance of the stellar component and the energy balance associated with the dissipation of gas turbulence and inflow down the potential gradient can lead to stabilization before $z = 0$.

This paper is organized as follows. In § 2 we introduce the ingredients of the model that describes the evolution of a self-regulated disc instability in a cosmological context. In § 3 we revisit the one-component case, separately for stars or gas, and introduce the fiducial model for a two-component disc of gas and stars. In § 4 we address the two-component evolution for values of the model parameters in a plausible range. In § 5 we discuss our results and draw conclusions.

Throughout the paper, we assume a flat Λ CDM cosmology specified by the cosmological parameters $(\Omega_m, \sigma_8, n, h) = (0.27, 0.81, 0.96, 0.70)$, motivated by the WMAP7+BAO+H0 results (Komatsu et al. 2011). The Hubble time in Gyr at redshift z is denoted by $t_H(z)$.

2 THE MODEL

We integrate in time the equations of mass and energy conservation under self-regulated, two-component disc instability. Before embarking on the details of the model, we present its three key components.

As a galactic disc of gas mass M_{gas} evolves, it obeys a simple *mass conservation* equation of the form

$$\dot{M}_{\text{gas}} = \dot{M}_{\text{source}} - \dot{M}_{\text{sink}}, \quad (1)$$

where \dot{M}_{source} is a given gas accretion rate of cosmological origin (§2.1.1), and the sink term consists of gas conversion into stars, gas inflow into the disc centre and possible mass expulsions in outflows. We assume that the sink term has the general form

$$\dot{M}_{\text{sink}} = M_{\text{gas}}/\tau, \quad (2)$$

where τ is a characteristic timescale. If \dot{M}_{source} and τ vary sufficiently slowly in time, then the equation converges on a timescale τ ($\propto e^{-t/\tau}$) to a steady-state solution where $\dot{M}_{\text{gas}} = 0$, $\dot{M}_{\text{source}} = \dot{M}_{\text{sink}}$, and $M_{\text{gas}} = \dot{M}_{\text{source}} \tau$. Analytic models based on variants of eq. (2) have been attempted for various purposes. Bouchè et al. (2010) and Krumholz & Dekel (2011) considered draining by star formation but ignored migration. On the other hand, DSC09 considered migration but ignored star formation and outflows. Davè et al. (2011) considered star formation and feedback as well as the return of outflowing gas back to the disc. Here, we consider the three sink terms of mass inflow towards the galaxy centre, star formation, and gas outflows due to stellar feedback.

A second important component in our model is the explicit appeal to *energy conservation* in the context of a self-regulated disc instability (§2.2). This is a new element in comparison to earlier studies (DSC09; Bouchè et al. 2010) and it is in line with the approach of Krumholz and Burkert (2010). At high redshift, galactic discs are expected to have a high surface density, reflecting the high mean cosmological density. The high gas accretion rate results in a high gas fraction, especially at $t < \tau$, when the sink term cannot yet catch up with the source term. Together, they lead to gravitational instability. In the perturbed discs, gravitational torques drive angular momentum out and thus cause mass inflow towards the centre, \dot{M}_{inflow} , (Gammie et al. 2002; DSC09; Krumholz and Burkert 2011; Bournaud et al. 2011). This inflow down the potential well between the disc outskirts and its centre, which is on the order of the circular velocity squared, V_{circ}^2 , provides an energy gain of $\dot{M}_{\text{inflow}} V_{\text{circ}}^2$, which can be used to stir up turbulence in the gas, characterized by a velocity dispersion σ_{gas} . Assuming that this energy gain roughly compensates for the dissipative losses of the turbulence, one can write

$$\dot{M}_{\text{inflow}} V_{\text{circ}}^2 \simeq \frac{M_{\text{gas}} \sigma_{\text{gas}}^2}{t_{\text{dis}}}. \quad (3)$$

Here, t_{dis} is the timescale over which the internal turbulent energy of the gas is dissipated. It is expected to be comparable to one or a few disc dynamical times, defined as $t_{\text{dyn}} = \Omega^{-1} = R_{\text{disc}}/V_{\text{circ}}$, where R_{disc} and Ω are the effective disc radius and angular velocity. The dissipation rate thus determines the disc inflow rate that is needed for self-regulating the disc instability at $Q \sim 1$.

The third key and new element of the model is the enforcement of self-regulated instability in a *two-component* disc made of gas and stars (§2.3). A disc is unstable once the self-gravitational attraction acting on a patch (associated with the surface density of cold material Σ) overcomes the repelling forces due to pressure (associated with σ) and rotation (associated with Ω) (Toomre 1964). This is expressed in terms of the Toomre parameter $Q \sim \sigma\Omega/\Sigma$

being smaller than unity. If the inflow in the disc is driven by the instability, and in turn it provides the power necessary for stirring up σ , the disc tends to self-regulate itself at $Q \sim 1$ as follows. When Q drops well below unity, because of a high Σ and/or a low σ , the disc becomes highly prerturbed, which increases the inflow rate. This depletes Σ and stirs up σ , pushing Q to above unity. As a result, the fragmentation stops, the inflow slows down, so Σ piles up by new accretion and σ cools down, driving Q to below unity, and so on. The new element incorporated in our current analysis is treating the instability in a disc made of two components, one dissipative and the other dissipationless, including the continuous conversion of gas to stars. The generalized instability analysis described in §2.3 refers to a two-component analog of the Toomre parameter, Q_{2c} , which is a function of the same Ω , the surface densities of the two components, and their different velocity dispersions, $\sigma_{\text{stars}} > \sigma_{\text{gas}}$. Since σ_{stars} cannot decrease and may actually increase in time, the maintenance of $Q_{2c} \sim 1$ has to rely on σ_{gas} being low. As the gas mass fraction in the disc gradually declines, σ_{gas} has to get lower and lower. However, when it becomes comparable to the thermal speed of sound, $c_s \sim 10 \text{ km s}^{-1}$, the pressure cannot keep decreasing as necessary, and Q is forced to be above unity. We refer to this as the end of the violent instability phase, or “stabilization”, and attempt to find out when it occurs for different choices of our model parameters.

2.1 Mass Conservation

Following eq. (1), the rate of change of gas mass in the disc is assumed to be given by

$$\dot{M}_{\text{gas,disc}} \simeq \dot{M}_{\text{gas,acc}} - \dot{M}_{\text{gas,inflow}} - \dot{M}_{\text{SFR}}(1 + \gamma_{\text{out}}). \quad (4)$$

Here, the source term, $\dot{M}_{\text{gas,acc}}$, is the gas supply rate into the disc. The sink term $\dot{M}_{\text{gas,inflow}}$ is the gas mass inflow rate in the disc towards the central bulge, which we sometimes loosely refer to as “migration”. The other sink term, \dot{M}_{SFR} , includes the star formation rate (SFR), and the outflow rate due to stellar feedback, which is assumed to be proportional to the SFR with γ_{out} a parameter of order unity. Similarly, the rate of change of disc stellar mass is

$$\dot{M}_{\text{star,disc}} \simeq \dot{M}_{\text{star,acc}} - \dot{M}_{\text{star,inflow}} + \dot{M}_{\text{SFR}}, \quad (5)$$

where $\dot{M}_{\text{star,acc}}$ represents the stellar fraction in the accretion rate into the disc, $\dot{M}_{\text{star,inflow}}$ is the stellar mass inflow rate within the disc, \dot{M}_{SFR} is the same as in eq. (4) but with an opposite sign, and the stars are assumed not to be affected by outflows. The rate of change of the total disc mass is the sum of (4) and (5). The source terms of accretion and the SFR are estimated as described below. Then, by appealing to energy conservation, gas-turbulence dissipation, and self-regulated instability, we will determine the inflow rates within the disc, and will be in a position to integrate eq. (4) and eq. (5).

For completeness, although we do not explicitly integrate it with time, we note that the growth of the central bulge is described by

$$\dot{M}_{\text{blg}} = \dot{M}_{\text{blg,mer}} + \dot{M}_{\text{bar,inflow}}, \quad (6)$$

where $\dot{M}_{\text{blg,mer}} = \dot{M}_{\text{bar}} - \dot{M}_{\text{gas,acc}} - \dot{M}_{\text{star,acc}}$ is the fraction of the total cosmological input of baryons that come in as big mergers that build the bulge without joining the disc, and $\dot{M}_{\text{bar,inflow}} = \dot{M}_{\text{gas,inflow}} + \dot{M}_{\text{star,inflow}}$ is the total baryon inflow rate within the disc (§2.1.1). We define the bulge-to-disk ratio as

$$B/D \equiv \frac{M_{\text{blg}}}{M_{\text{star,disc}} + M_{\text{gas,disc}}}. \quad (7)$$

Following DSC09, we appeal to the convenient parameter δ_{disc} , the fraction of mass in the disc component within the characteristic radius of the disc, R_{disc} ,

$$\delta_{\text{disc}} \equiv \frac{M_{\text{star,disc}} + M_{\text{gas,disc}}}{M_{\text{tot}}}. \quad (8)$$

Here the total mass M_{tot} within R_{disc} includes the contributions of gas and stars in the disc, the stellar bulge, and the dark matter within R_{disc} . The maximum possible value of δ is β , the fraction of baryons including disc and bulge within the disc radius,

$$\delta_{\text{disc}} \leq \beta \equiv \frac{M_{\text{bar}}}{M_{\text{tot}}}. \quad (9)$$

The ratio of disc to total baryonic mass is then $M_{\text{disc}}/M_{\text{bar}} = \beta^{-1}\delta_{\text{disc}}$, so that a bulge-less disc corresponds to $\delta_{\text{disc}} = \beta$, and a disc-less bulge is $\delta_{\text{disc}} = 0$. The bulge-to-disc ratio is $B/D = (\beta - \delta_{\text{disc}})/\delta_{\text{disc}}$. For gas and stars separately, we have

$$\delta_{\text{gas}} \equiv \frac{M_{\text{gas,disc}}}{M_{\text{tot}}} \quad \text{and} \quad \delta_{\text{star}} \equiv \frac{M_{\text{star,disc}}}{M_{\text{tot}}}, \quad (10)$$

with $\delta_{\text{disc}} = \delta_{\text{gas}} + \delta_{\text{star}}$. In order to estimate the value of β , following DSC09, we crudely treat the halo as an isothermal sphere with a mass profile $M(r) \propto r$, so we can write $M_{\text{tot}} \simeq \lambda M_{\text{vir}} + M_{\text{bar}}$, where λ is the halo spin parameter, M_{vir} is the halo virial mass, and M_{bar} is the baryonic mass. This leads to $\beta \simeq f_{\text{bar}}/(f_{\text{bar}} + \lambda)$, where f_{bar} is the baryonic mass fraction within the virial radius (which could be lower than the universal fraction due to mass loss in outflows). Throughout the paper we assume $\lambda = 0.05$, $f_{\text{bar}} = 0.075$, and thus $\beta = 0.6$.

2.1.1 Cosmological Gas Supply

Both analytic estimates and cosmological simulations predict that the cosmological baryonic input funnels into high-redshift galaxies through cold streams that follow the filaments of the cosmic web and include merging galaxies and a smoother component (e.g., Birnboim & Dekel 2003; Keres et al. 2005; Dekel & Birnboim 2006; Ocvirk et al. 2008; Dekel et al. 2009). The average baryon input rate is well approximated by the universal baryon fraction times the total cosmological input rate into galactic haloes (Dekel et al. 2009). We estimate the corresponding timescale for accretion into a halo of mass M_{vir} at redshift z by

$$t_{\text{acc}} \equiv \frac{M_{\text{vir}}}{\dot{M}_{\text{vir}}} \simeq 2.1 (1+z)_3^{-2.4} M_{12}^{-0.14} \text{ Gyr}, \quad (11)$$

where $(1+z)_3 \equiv (1+z)/3$ and $M_{12} \equiv M_{\text{vir}}/10^{12} M_{\odot}$. This approximation for the average specific accretion rate has been derived by fine tuning an analytic prediction based on the EPS approximation (Neistein et al. 2006), and it has been shown to fit well the halo growth rate measured in the Millennium cosmological N-body simulation (Neistein et al. 2008; Genel et al. 2008; Fakhouri et al. 2010), except that the numerical coefficient and the powers in eq. (11) were slightly adjusted for the WMAP7 cosmological parameters used here. Eq. (11) is accurate to better than 5% in the redshift range $0.2 < z < 5$, and is an underestimate of $\approx 10\%$ at $z = 0$ and $z = 10$.

The analytic EPS prediction in the high-redshift Einstein-deSitter cosmological regime is actually $\dot{M} \propto (1+z)^{5/2}$. This is a good approximation at $z > 1$, where the redshift is related to the Hubble time in Gyr as $(1+z) \simeq 6.6t^{-2/3}$. For the purpose of a toy model that will turn out useful for back-of-the-envelope estimates, we tentatively ignore the weak mass dependence of eq. (11), and keep the same specific accretion rate for $M_{12} = 0.56$ at

$(1+z) = 3$. By integrating eq. (11), such a halo ends up as a Milky-Way halo with $M_{12} = 2$ at $z = 0$, which is comparable to the final mass of the halo used in our fiducial model below. The toy-model version of eq. (11) becomes

$$\frac{\dot{M}}{M} \simeq A(1+z)^{5/2}, \quad A \simeq 0.028 \text{ Gyr}^{-1}. \quad (12)$$

This implies a simple expression for the halo and galaxy mass growth,

$$M \propto e^{-\alpha z}, \quad (13)$$

with $\alpha \simeq 25.4 A \simeq 0.72$. A similar exponential growth has been found using cosmological N-body simulations (Wechsler et al. 2002).

In our model, we assume that a fraction γ_{acc} of the average baryonic mass input rate actually joins the disc as gas. This is a multiple of two factors, (1) the fraction of the baryonic input in smooth accretion including small mergers that join the rotating disc, as opposed to more massive mergers that build the bulge, and (2) the fraction of gas in this smoother component, as opposed to stars that come in with small merging galaxies and also join the disc. We thus write for the specific gas accretion rate into the disc

$$\left. \frac{\dot{M}_{\text{bar,acc}}}{M_{\text{bar}}} \right|_{R_{\text{disc}}} \simeq \gamma_{\text{acc}} t_{\text{acc}}^{-1} \equiv t_{\text{disc,acc}}^{-1}. \quad (14)$$

We test the effects of varying γ_{acc} about a fiducial value of $\gamma_{\text{acc}} = 0.7$. This is based on the estimate of D09 from hydro cosmological simulations that the average fraction of incoming mass in clumps that lead to mergers with a mass ratio larger than 1:10 is about 30%.

We have made so far three simplifying assumptions that are worth mentioning. First, we limit the current analysis to the simple case of accretion at the average cosmological rate. In reality, the accretion rate is varying, both among different galaxies and along the history of each galaxy. The effects of these variations in the accretion rate will be studied in a follow-up paper. Second, the accretion rate onto galaxies may be sensitive to uncertain feedback processes, perhaps more important at lower redshifts (e.g., van de Voort et al. 2010). A detailed modeling of this is beyond the scope of this paper. Third, a fraction of the accreting mass into the disc is expected to be already in stars, formed earlier in small merging galaxies (e.g., D09; Ceverino, Dekel & Bournaud 2010). These stars could partly contribute to a “cold” stellar component that would participate in the gravitational disc instability and partly to a “hot” stellar component, equivalent to the bulge in terms of its effect on the disc instability. In our current application we do not explicitly account for the stars that accrete onto the cold disc, and absorb the corresponding uncertainty in the value of γ_{acc} , assumed to represent the fraction of mass that accretes onto the disc, all in gas.

2.1.2 Star Formation & Outflows

As summarized in Krumholz, Dekel & McKee (2011) and references therein, stemming from the Kennicutt-Schmidt empirical SFR law (e.g., Kennicutt 1998), the star formation rate can be best modeled by a universal volumetric local star formation law. When expressed in terms of surface densities it has the form

$$\dot{\Sigma}_{\text{SFR}} \equiv \frac{\Sigma_{\text{gas}}}{\tau_{\text{SFR}}} = \epsilon_{\text{sfr}} \frac{\Sigma_{\text{gas}}}{t_{\text{ff}}}, \quad (15)$$

where $\dot{\Sigma}_{\text{SFR}}$ is the SFR surface density, Σ_{gas} is the mass surface density of molecular gas, and $t_{\text{ff}} = [3\pi/(32G\rho)]^{1/2}$ is the local

free-fall time in the star forming region, derived from the local volumetric mass density ρ . The dimensionless parameter ϵ_{sfr} is the SFR efficiency, i.e., the fraction of gas that is transformed into stars per free-fall time, and has been argued based on theory and observations to be constant in all star forming regions, at the level of 1 to a few percent. In high redshift discs that are self-regulated at a Toomre instability with $Q \sim 1$, the free-fall time in the giant clumps where stars form are comparable to the global disc crossing time t_{dyn} , the inverse of the disc angular velocity $\Omega = V_{\text{circ}}/R_{\text{disc}}$, which is comparable to its vertical crossing time (Krumholz, Dekel & McKee 2011).

In a variant of eq. (15), Krumholz et al. (2009, hereafter K09) have argued that the physics of star formation within a molecular cloud, and in particular the variation in t_{ff} , can be encapsulated in the following star formation law

$$\dot{\Sigma}_{\text{SFR}} = \frac{\Sigma_{\text{gas}}}{2.6 \text{ Gyr}} \times \begin{cases} \Sigma_{\text{gas},85}^{-0.33} & \text{if } \Sigma_{\text{gas},85} < 1 \\ \Sigma_{\text{gas},85}^{+0.33} & \text{if } \Sigma_{\text{gas},85} > 1, \end{cases} \quad (16)$$

where $\Sigma_{\text{gas},85} = \Sigma_{\text{gas}}/(85M_{\odot} \text{ pc}^{-2})$. The origin of these two regimes is that clumps in discs with $\Sigma_{\text{gas},85} > 1$ are in the regime where they have the characteristic Toomre mass, while in galaxies of lower surface density the clumps collapse and fragment until they reach the critical surface density of $85M_{\odot} \text{ pc}^{-2}$ that characterize low-redshift molecular clouds. The galactic discs at high redshift are practically always in the regime where $\Sigma_{\text{gas},85} > 1$ while at low redshift they enter the other regime. In relatively massive, metal rich discs, the gas in the disc can be assumed to be all molecular, while in less massive discs, especially at high redshift, the molecular gas fraction becomes smaller than unity and should be considered when deriving the molecular surface density from the total gas surface density (Krumholz & Dekel 2011).

Outflows due to stellar feedback are incorporated in eq. (4) through the term

$$\dot{M}_{\text{out}} = \gamma_{\text{out}} \dot{M}_{\text{SFR}} \quad (17)$$

with γ_{out} assumed to be of order unity and constant with time (see Table 2). This parameterization is based on theoretical and observational results (Bouché et al. 2006; 2007; 2009; Martin & Bouché 2009). While this takes into account the important role of feedback in removing gas from the disc, we assume that the contribution of feedback to stirring up gas turbulence on galactic scales is minor (Joung et al. 2009; Ostriker & Shetty 2011; but see also Hopkins et al. 2011).

2.2 Energy Conservation

The gravitational instability in the disc is associated with torques that drive an outward angular-momentum flux and a corresponding mass inflow towards the disc centre (Gammie 2001; DSC09; Krumholz & Burkert 2010; Bournaud et al. 2011). This inflow involves both the gas and the stars, in the form of clump migration as well as inflow of the smoother material in the disc outside the clumps. We assume that the gravitational energy released by this mass inflow down the potential well, at a rate $\dot{E}_{\text{gas,inflow}} + \dot{E}_{\text{star,inflow}}$, is deposited in the velocity dispersions of the two disc components. This is a “gravitational heating” effect (Birnboim & Dekel 2008; Khochfar & Ostriker 2008). While the stellar component does not dissipate the acquired energy, the internal energy of the gas component dissipates on the turbulence dissipation timescale at a rate \dot{E}_{dis} . This is summarized in an energy conservation equation for the disc internal energy,

$$\dot{E}_{\text{disc,int}} = \dot{E}_{\text{gas,inflow}} + \dot{E}_{\text{star,inflow}} - \dot{E}_{\text{dis}}. \quad (18)$$

In order to solve our system of equations, we need to use an additional physical constraint. Here we make the strong assumption, that the inflow velocities of the gas and stars are the same, and that the energy gain is split between the two components in proportion to their masses. An example of stellar inflow is the clumps migration, but the inter-clump stars are also flowing in. Such a behavior is indicated in zoom-in cosmological simulations (Cacciato et al., in preparation), but for now it should be considered a working assumption, to be fine-tuned later. This assumption allows us to split the energy equation into two,

$$\dot{E}_{\text{gas,int}} = \dot{E}_{\text{gas,inflow}} - \dot{E}_{\text{dis}} - \dot{E}_{\text{SFR}} \quad (19)$$

$$\dot{E}_{\text{star,int}} = \dot{E}_{\text{star,inflow}} + \dot{E}_{\text{SFR}}, \quad (20)$$

where $\dot{E}_{\text{gas,int}}$ and $\dot{E}_{\text{star,int}}$ represent the rate of change of internal energy for gas and stars, respectively, and \dot{E}_{SFR} refers to the energy transfer between the two components as gas turns into stars.

The gravitational potential difference between the outer disc edge and the disc centre is of order V_{circ}^2 . We then rewrite the energy equations as

$$\frac{3}{2} \frac{d(M_{\text{gas}} \sigma_{\text{gas}}^2)}{dt} \approx V_{\text{circ}}^2 \dot{M}_{\text{gas,inflow}} - \frac{3}{2} M_{\text{gas}} \sigma_{\text{gas}}^2 (t_{\text{dis}}^{-1} - \tau_{\text{SFR}}^{-1}) \quad (21)$$

$$\frac{3}{2} \frac{d(M_{\text{star}} \sigma_{\text{star}}^2)}{dt} \approx V_{\text{circ}}^2 \dot{M}_{\text{star,inflow}} + \frac{3}{2} \frac{M_{\text{gas}} \sigma_{\text{gas}}^2}{\tau_{\text{SFR}}}. \quad (22)$$

The internal velocity is associated with a one-dimensional gas velocity dispersion σ_{gas} . It consists of a contribution from turbulence, σ_{turb} , and from thermal energy, through the speed of sound c_s , $\sigma_{\text{gas}}^2 = c_s^2 + \sigma_{\text{turb}}^2$. We assume that $c_s \simeq 10 \text{ km s}^{-1}$, corresponding to gas cooled by atomic cooling to 10^4 K .

The turbulence dissipation timescale in eq. (21) is parametrized as proportional to the disc vertical crossing time, which for $Q \sim 1$ is comparable to the crossing time in the disc plane, namely

$$t_{\text{dis}} = \gamma_{\text{dis}} t_{\text{dyn}}. \quad (23)$$

The value of γ_{dis} is expected to be about unity if the turbulence lengthscale ℓ_{turb} is comparable to the disc scale height h_{disc} or smaller, while it could be somewhat larger, $\gamma_{\text{dis}} \simeq \ell_{\text{turb}}/h_{\text{disc}}$, if there is turbulence on scales larger than h_{disc} . We adopt $\gamma_{\text{dis}} = 3$ as our fiducial value, and study the effect of vaying this parameter between 1 and 10 in § 4.1.

Three further comments are in place regarding the energy equations. First, since the star formation timescale is two orders of magnitude larger than the dynamical timescale, the dissipation term dominates the right hand side of eq. (21). Thus, as long as the internal energy of the gas is varying slowly, eq. (21) is approximated by eq. (3), where the gas inflow rate is determined by the dissipation rate, with only a minor correction due to the presence of the stellar component. Second, when the turbulence becomes very weak with a small σ_{turb} , the dissipation timescale becomes much longer than the dynamical time, and the inflow rate slows down accordingly. In our simple model we do not explicitly incorporate this effect, and instead consider the time at which σ_{gas} becomes as small as c_s as the time of “stabilization”, which we term z_{stab} . Third, in eq. (22), the change in the stellar internal energy is assumed to consist of two terms. The second term represents the addition of newly born stars with a velocity dispersion that equals the instantaneous gas velocity dispersion, while the first term corresponds to the gravitational “heating” of the stars by the stellar mass inflow in the disc. It

is worth recalling that the stellar heating rate is determined by the assumption that the disc stars flow in with the same velocity as the gas.

2.3 Two-Component Gravitational Instability

According to the standard *one-component* Toomre instability analysis (Toomre 1964), a thin rotating disc of gas or stars becomes unstable to axisymmetric modes once the attraction due to self-gravity, represented by the surface density Σ , overcomes both the centrifugal force due to rotation and the pressure force associated with the radial velocity dispersion σ . For gas, there is an additional contribution from thermal pressure, but the high-redshift discs under investigation here are in a regime where the velocity dispersion associated with turbulence is larger than the speed of sound that characterizes the thermal pressure. The instability is expressed in terms of the condition that the Toomre parameter Q is smaller than a critical value Q_{crit} of a value about unity (Toomre 1964),

$$Q = \frac{\sigma \kappa}{\pi G \Sigma} < Q_{\text{crit}} \simeq 1. \quad (24)$$

Here κ is the epicyclic frequency, related to the angular circular velocity $\Omega(r)$ by $\kappa^2 = r d\Omega^2/dr + 4\Omega^2$. For a power-law rotation curve $V_{\text{circ}} \propto r^\nu$, this becomes $\kappa^2 = 2(1 + \nu)\Omega^2$. We adopt here a flat rotation curve, as seen in cosmological simulations, namely $\nu = 0$. We adopt an effective value $\Omega = V_{\text{circ}}/R_{\text{disc}}$, where the circular velocity is approximated by the virial velocity, and the disc radius is a constant fraction of the virial radius, $R_{\text{disc}} = \lambda R_{\text{vir}}$, with $\lambda = 0.05$ representing the halo spin parameter. Thus, the time evolution of κ depends only on the cosmological evolution of the halo virial quantities (see § 3). For a thin disc, gaseous or stellar, $Q_{\text{crit}} \simeq 1$. For a thick disc, the Toomre analysis is valid as long as the length scale of the perturbation is larger than the disc thickness and smaller than the disc radius, with $Q_{\text{crit}} \approx 0.67$ (Goldreich & Lynden-Bell 1965).

When the disc is made of two components, gas and stars, each with different Σ and σ , one can address the axisymmetric instability via a two-dimensional Toomre-like parameter Q_{2c} which can be expressed in terms of Q_{star} and Q_{gas} , each defined by eq. (24) with the Σ and σ of the corresponding component (Jog & Solomon 1984; Romeo 1994; Wang & Silk 1994; Rafikov 2001). The difference in the expression for Q_{2c} due to the dissipative nature of the gas is small when we focus attention to the most unstable scale (Rafikov 2001), and we ignore it here. Romeo & Wiegert (2011) proposed the convenient expression that we use here,

$$Q_{2c}^{-1} = \begin{cases} W Q_{\text{star}}^{-1} + Q_{\text{gas}}^{-1} & \text{if } Q_{\text{star}} > Q_{\text{gas}} \\ Q_{\text{star}}^{-1} + W Q_{\text{gas}}^{-1} & \text{if } Q_{\text{star}} < Q_{\text{gas}}, \end{cases} \quad (25)$$

where

$$W = \frac{2\sigma_{\text{star}}\sigma_{\text{gas}}}{\sigma_{\text{star}}^2 + \sigma_{\text{gas}}^2}. \quad (26)$$

Two-component instability is characterized by $Q_{2c} \leq 1$. The parameter Q_{2c} can be thought of as a combination of Q_{star} and Q_{gas} , weighted by a function of the ratio of the velocity dispersions of gas and stars.

In order to account for a disc thickness, associated with a vertical velocity dispersion $\sigma_{i,z}$ for the i 's component (gas or stars), the quantities that enter eq. (25) are $Q_i = T_i Q_i$, with the approximation $T_i \simeq 0.8 + 0.7(\sigma_{i,z}/\sigma_i)$ valid for $0.5 < \sigma_{i,z}/\sigma_i < 1$ (Romeo & Wiegert 2011; Romeo 1994). Setting T_i to unity corresponds to a thin disc in that component. Here we adopt disc thicknesses that

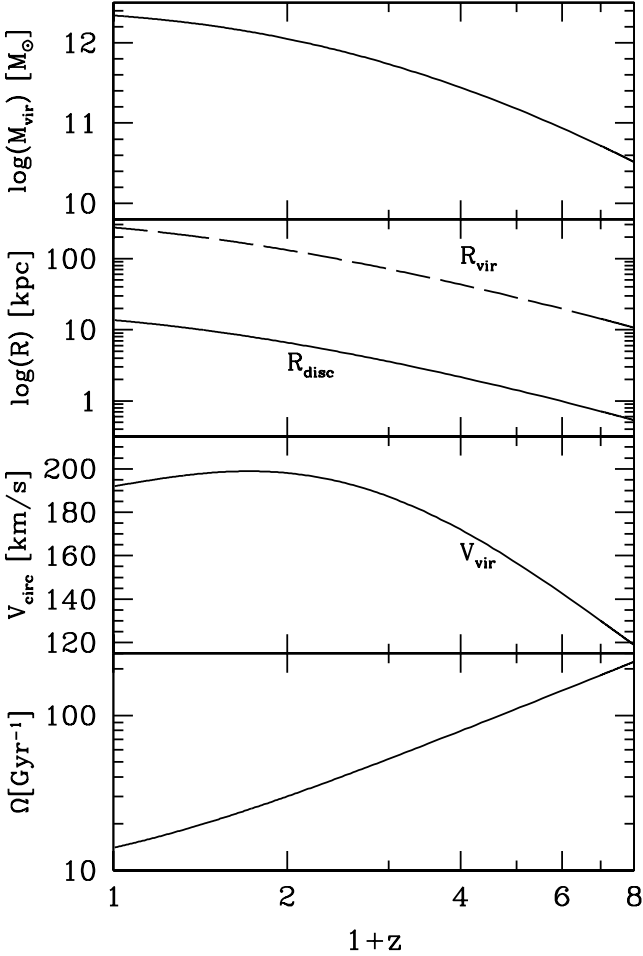


Figure 1. Cosmological evolution of the global quantities in our fiducial model galaxy. Shown from top to bottom are (a) the halo virial mass M_{vir} , (b) the virial and disc radius, R_{vir} and $R_{\text{disc}} = \lambda R_{\text{vir}}$, with $\lambda = 0.05$, (c) the circular velocity V_{circ} , assumed equal to the virial velocity V_{vir} , and (d) the angular velocity $\Omega = V_{\text{circ}}/R_{\text{disc}}$, which at high redshift is inversely proportional to the cosmological time.

are determined by the assumption of isotropic velocity dispersion for each component, $\sigma_{i,z} = \sigma_i$. As a sanity check, note that under this assumption $Q_i = 1$ corresponds to $Q_i \approx 0.67$, in agreement with the original result for a one-component thick disc (Goldreich & Lynden-Bell 1965).

Note that the two-component system can be unstable, $Q_{2c} \leq 1$, even when each of the components has $Q_i > 1$. For instance, in the thin-disc approximation, with the gas and stars having the same σ_i and the same Σ_i , $Q_{2c} = 1$ corresponds to $Q_i = 2$ for each of the components.

3 MODEL PREDICTIONS

In the current paper we focus on a halo that grows by the average cosmological growth rate, eq. (11), into a halo comparable to the Milky Way halo with $M_{12} = 2$ at $z = 0$. The virial relations between the halo virial mass, velocity and radius are

$$V_{\text{vir}}^2 = \frac{GM_{\text{vir}}}{R_{\text{vir}}}, \quad \frac{3M_{\text{vir}}}{4\pi R_{\text{vir}}^3} = \Delta \bar{\rho}, \quad (27)$$

where $\bar{\rho}$ is the average mass density of the universe at that time. In the Λ CDM cosmology, they can be expressed as

$$M_{12} \approx 0.6V_{100}^3 A^{3/2} \approx 34.2R_1^3 A^{-3}, \quad (28)$$

where $V_{100} \equiv V_{\text{vir}}/100$ km/s, $R_1 \equiv R_{\text{vir}}/1$ Mpc, and A is the modified expansion factor,

$$A \equiv a \left[\frac{\Delta}{200} \frac{\Omega_m}{0.3} \left(\frac{h}{0.7} \right)^2 \right]^{-1/3}, \quad (29)$$

with $a = 1/(1+z)$. The cosmological time evolution of the density parameter Ω_m and the Hubble constant, $h = H_0/100$ km s $^{-1}$ Mpc $^{-1}$, is given by

$$\Omega_m(a) = \frac{\Omega_m a^{-3}}{\Omega_\Lambda + \Omega_m a^{-3}}, \quad H(a) = H_0 (\Omega_\Lambda + \Omega_m a^{-3})^{1/2}, \quad (30)$$

and we use the approximation proposed by Bryan & Norman (1998) for the cosmological time dependence of Δ :

$$\Delta = 18\pi^2 - 82\Omega_\Lambda - 39\Omega_\Lambda^2. \quad (31)$$

The halo mass growth is shown in the top panel of Fig. 1. It roughly follows the approximation eq. (13), reaching $M_{12} \simeq 0.5$ at $z = 2$ and $M_{12} \simeq 1$ at $z = 1$.

The second panel of Fig. 1 shows the corresponding R_{vir} and $R_{\text{disc}} = \lambda R_{\text{vir}}$ with $\lambda = 0.05$. The third panel of Fig. 1 shows the evolution of the corresponding disc circular velocity, which we assume equals the virial velocity. This velocity is growing with time to a flat maximum at $z \simeq 1.1$, followed by a gradual decline towards $z = 0$. This can be reproduced with the mass growing as in the approximation eq. (13),

$$V_{\text{vir}} \propto (1+z)^{1/2} \exp(-\alpha z/3). \quad (32)$$

This indeed reaches a maximum at $z_{\text{max}} \simeq 3/(2\alpha) - 1 \simeq 1.1$. We will see below that this governs the evolution of σ in the one-component case, and that it also has an important effect on the evolution of the velocity dispersions in the two-component case, partly through the dependence of the gravitational heating on the potential well expressed by V_{circ} .

The bottom panel of Fig. 1 shows the angular velocity Ω , which enters in the instability Q parameter. Recall that $\Omega = t_{\text{dyn}}^{-1}$. In the Einstein deSitter phase where Δ_{vir} is constant, and under the assumption of a constant spin parameter λ , t_{dyn} is proportional to the cosmological time¹.

3.1 A one-component disc

As a first application of our model, we investigate the evolution of instability in a one-component disc. Isolating σ from eq. (24), we can write for a disc with a flat rotation curve

$$\sigma = \frac{\pi G \Sigma_{\text{disc}} Q_{\text{crit}}}{\sqrt{2}\Omega} = \frac{1}{\sqrt{2}} \delta_{\text{disc}} V_{\text{circ}} Q_{\text{crit}}. \quad (33)$$

Inserting this expression for σ in the mass and energy equations, we can straightforwardly integrate them.

Fig. 2 shows the evolution of a one-component disc for different values of the dissipation parameter γ_{dis} (eq. (23)). A choice of $\gamma_{\text{dis}} \sim \infty$ refers to a dissipationless, all stellar disc. The finite

¹ For the standard Λ CDM cosmology, in its Einstein-de Sitter regime, the virial radius and velocity are related to the virial mass as $R_{\text{vir}} \sim 308$ kpc $(1+z)^{-1} M_{12}^{1/3}$ and $V_{\text{vir}} \sim 118$ km/s $(1+z)^{1/2} M_{12}^{1/3}$. Thus $V_{200} \sim R_{100}(1+z)^{3/2}$, where the quantities are in units of 200 km/s and 100 kpc.

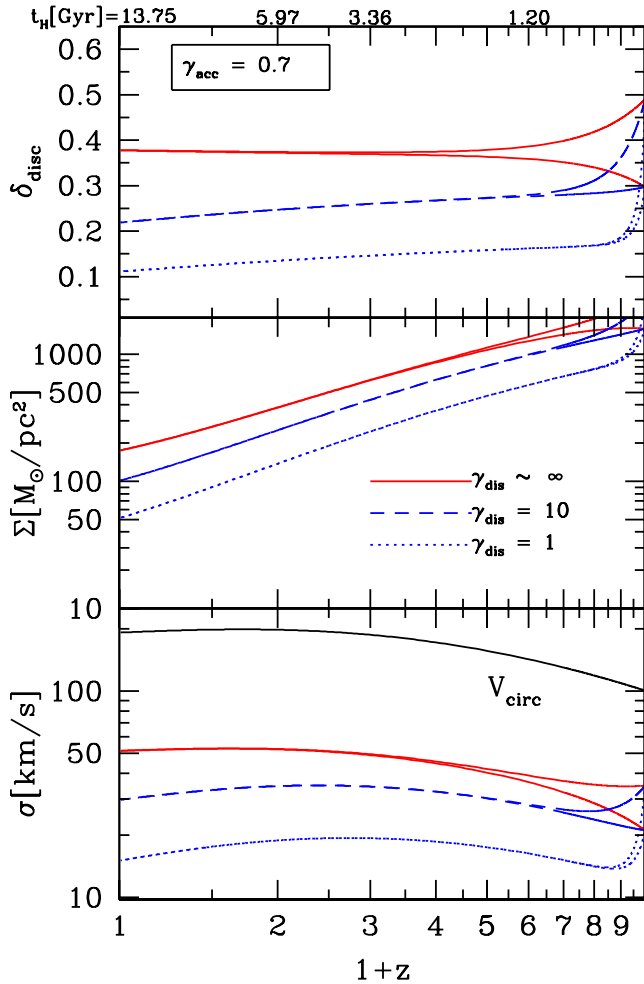


Figure 2. Evolution of a one-component disc and the role of dissipation. Red solid lines refer to non-dissipative stellar discs, and blue dashed and dotted lines refer to gaseous discs with $\gamma_{\text{dis}} = 10$ and 1, respectively. *Top:* Mass fraction in the disc within R_{disc} , $\delta_{\text{disc}} \simeq \sqrt{2}\sigma/V_{\text{circ}}$. *Middle:* Disc surface density Σ . *Bottom:* Velocity dispersion σ and V_{circ} for comparison. Lower γ_{dis} , corresponding to a higher dissipation rate, requires a lower velocity dispersion for maintaining $Q \simeq 1$.

values of γ_{dis} in the range 10-1 correspond to a pure gaseous disc with slow and rapid dissipation, $\gamma_{\text{dis}} = 10, 1$ respectively. For each choice of γ_{dis} we show the results for two different initial conditions, which practically converge to a single solution by $z \sim 5$, in accordance with the exponential convergence described in §2.

The top panel of Fig. 2 shows the time evolution of the disc mass fraction, δ_{disc} , which in the one-component analysis is $\sqrt{2}Q_{\text{crit}}(\sigma/V_{\text{circ}})$. We see that δ_{disc} is roughly constant in time, or is varying rather slowly, indicating that the system evolves in a quasi-steady-state, where the disc and the bulge grow together, as emphasized in DCS09. In the case of a stellar disc, the disc fraction is high, $\delta_{\text{disc}} \approx 0.4$, close to the maximum possible value of $\beta = 0.6$, namely a bulge-to-disc ratio of 0.5. This reflects the fact that without dissipation the inflow rate in the disc is rather slow, eq. (3). For lower values of γ_{dis} , the disc fraction δ_{disc} becomes lower, reflecting the higher depletion rate by inflow when the dissipation is faster. With $\gamma_{\text{dis}} = 10$, the steady-state is with $\delta_{\text{disc}} \simeq 0.25$, namely B/D $\simeq 1.4$, and with $\gamma_{\text{dis}} = 1$ it is $\delta_{\text{disc}} \simeq 0.15$, corresponding to B/D ~ 3 .

Table 1. One-Component Models

	γ_{dis}	γ_{acc}	τ_{SFR}	γ_{out}
Dissipation	$\sim \infty$	0.7	–	0
	10	0.7	–	0
	1	0.7	–	0

The middle panel of Fig. 2 shows how Σ_{disc} is gradually decreasing with time. This reflects the assumptions that the galaxy mass follows the halo mass growth, that is close to exponential following eq. (13), and that the galaxy size is a constant fraction of the virial radius. Then, according to the approximate behavior of eq. (13) and in the Einstein-deSitter regime with a constant λ , the three-dimensional density is proportional to the virial density, namely it is independent of mass and follows the cosmological density evolution. We thus have:

$$\Sigma \propto \frac{M}{R^2} \propto \delta_{\text{disc}} (1+z)^2 \exp(-\alpha z/3). \quad (34)$$

For a slowly varying δ_{disc} , as seen in the top panel of Fig. 2, and for $\alpha \simeq 0.72$ as in eq. (13), the surface density of eq. (34) is indeed decreasing with time at all redshifts $z < 7.4$, namely throughout most of the relevant redshift range.

The lower panel of Fig. 2 shows the evolution of the velocity dispersion in the one-component models, with V_{circ} shown as a reference. Based on eq. (33), σ is determined by Σ/Ω , or equivalently by $\delta_{\text{disc}} V_{\text{circ}}$. Since δ_{disc} is rather constant, σ is roughly proportional to V_{circ} , which follows the evolution of the virial velocity shown in Fig. 1 and approximated in eq. (32). This explains why σ is rising to a flat maximum near $z \sim 1$ and is gradually declining afterwards. Thus, the evolution of σ is driven by the cosmological halo growth rate and the evolution of its virial velocity. More precisely, the evolution of σ is determined by the interplay between the rates of change of Σ and Ω under the constraint that $Q \simeq 1$ (eq. (24)). Figure 3 demonstrates this, and in particular the qualitative role played by the sink terms in causing the decline of σ at late times. The top panel shows a simplified model in which mass accretes onto the disk in the average cosmological rate, but the sink terms are all turned off, $\delta_{\text{disc}} = \text{const.}$, and there is no dissipation. In this case, the evolution of Σ and Ω are dictated solely by the cosmological evolution of the virial quantities, under the assumption of a constant spin parameter and $V_{\text{circ}} = V_{\text{vir}}$. We note that in this case, in the redshift range $z = 3 - 0$, that the decline rate of Σ and Ω are quite similar, so σ maintains a rather constant value. The toy model of eq. (13), in the Einstein-deSitter regime, indeed predicts a slow evolution $\sigma \propto \Sigma/\Omega \propto (1+z)^{1/2} e^{-0.24z}$. The bottom panel of Fig. 3 refers to the same model but with an artificial suppression term ($\propto (1+z)^{1/2}$). In this case, at late times, Σ drops in time faster than Ω , so σ has to decline in order to maintain $Q \sim 1$, as it does in Fig. 2.

For the models shown in Fig. 2, we see that self-regulated instability is maintained till $z = 0$, in the sense that the model has $\sigma_{\text{gas}} > c_s \simeq 10 \text{ km s}^{-1}$ at all times, even for the case in which the dissipation rate is as high as the disc crossing time. This result is consistent with the analysis of DSC09, who concluded that an unstable disc accreting at the average cosmological rate remains unstable throughout its cosmic history.

We note that DSC09 estimated the migration timescale via an explicit calculation of the effect of encounters between giant clump,

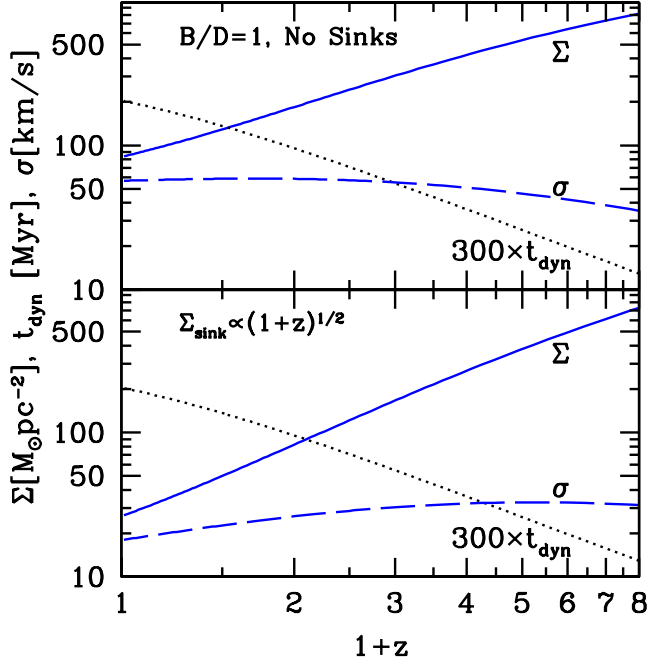


Figure 3. An illustration of the way the velocity dispersion compensates for the rate of change of Σ/Ω to keep $Q \sim 1$. *Top*: a case where the disc grows by cosmological accretion but all sink terms are turned off, showing $\sigma \propto \Sigma/\Omega \simeq \text{const.}$. *Bottom*: the same but with an arbitrary sink term added, showing a decline of σ in the regime where Σ/Ω declines, similar to Fig. 2.

Table 2. Two-Component Models

	γ_{dis}	γ_{acc}	τ_{SFR}	γ_{out}
Fiducial	3	0.7	K09	0
Gas Dissipation	10	0.7	K09	0
	1	0.7	K09	0
Gas Accretion	3	1	K09	0
	3	0.4	K09	0
Star Formation	3	0.7	$\tau_{\text{dyn}}/0.01$	0
	3	0.7	$\tau_{\text{dyn}}/0.05$	0
Outflows	3	0.7	K09	1
	3	0.7	K09	3
Extreme	1	0.4	K09	3

and alternatively via torques in a viscous disc, without considering the energy budget. In Fig. 4 we show that our current model, based on energy considerations, without specifying the mechanism by which this energy is transferred to velocity dispersion and to inflow in the disc, predicts an inflow timescale similar to the estimate in DSC09. This agreement is non-trivial given the fundamental difference between the two calculations. We also see that the two calculations predict inflow timescales that are comparable to the accretion timescale.

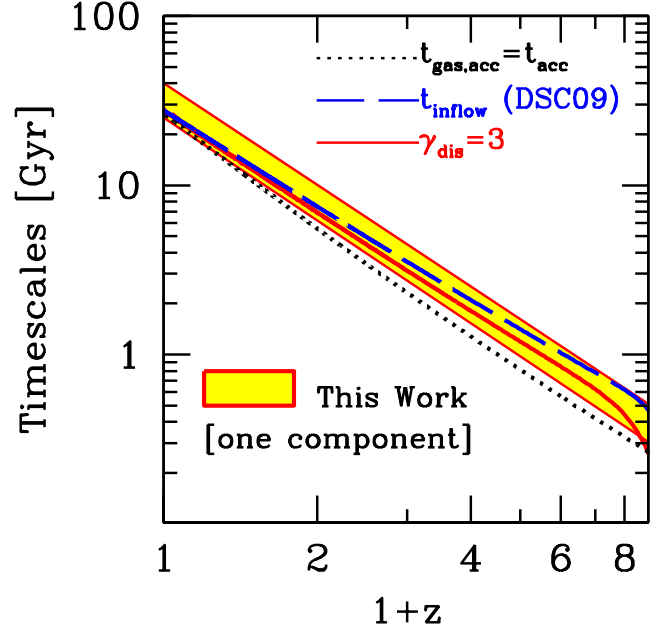


Figure 4. Evolution of relevant timescales, showing the cosmological accretion timescale (black dotted line), the timescale for mass inflow in the disc as derived by DSC09 from clump interactions and torques (blue dashed line), the timescale for mass inflow in the disc according to our fiducial model (red solid line), and its range corresponding to variations in γ_{dis} in the range (1, 10) (yellow shaded area).

3.2 Disc of Gas and Stars: Fiducial Model

After recovering the persistence of instability in the one-component models, we proceed to the two-component case. Here, the gas fraction in the disc is gradually declining with time, which may lead to stabilization once the disc becomes dominated by a hot stellar component. In this section, we describe the results for a specific set of model parameters, which we refer to as the fiducial model. In §4 we will address the effects of varying the model parameters about the fiducial values.

Our fiducial model, as specified in Table 2, consists of $\gamma_{\text{dis}} = 3$ (eq. (23)), $\gamma_{\text{acc}} = 0.7$ (eq. (14)), the K09 star formation law (eq. (16)), and tentatively $\gamma_{\text{out}} = 0$ (eq. (17)). Fig. 5 shows the time evolution of the same quantities shown in Fig. 2, namely δ_{disc} , Σ and σ , but now, and in the following figures, referring to the two components of gas and stars in blue and red respectively, and to their sum in black. We immediately note in the bottom panel that, unlike the always-unstable one-component models, the fiducial two-component model does stabilize shortly prior to $z = 0$, at $z \simeq 0.15$, as marked by σ_{gas} dropping below $c_s = 10 \text{ km s}^{-1}$. The drop is rather steep, starting at $z \sim 1$ after a pretty constant $\sigma_{\text{gas}} \simeq 30 \text{ km s}^{-1}$ till then. It is driven by the disc turning from being gas dominated at early times to star dominated at $z \simeq 1.5$, as seen in the top and middle panels, with $\Sigma_{\text{star}}/\Sigma_{\text{gas}} \simeq \delta_{\text{stars}}/\delta_{\text{gas}} \simeq 5$ by $z = 0.15$. With the stars “hot” at $\sigma_{\text{star}} \simeq 80 - 100 \text{ km s}^{-1}$ in the range $z \sim 1 - 0$, the gas has to cool faster than in the one-component case in order to compensate for its decreasing fraction in the disc surface density and keep $Q_{2c} = 1$.

We note several additional interesting features in the evolution of the fiducial model compared to the one-component models. First, the gas velocity dispersion is at the level of $\sigma_{\text{gas}} \simeq 30 \text{ km s}^{-1}$ until it starts dropping at $z \sim 1$. At $z = 2$ this corresponds to $V_{\text{circ}}/\sigma_{\text{gas}} \sim 6.6$, reaching $V_{\text{circ}}/\sigma_{\text{gas}} \simeq 10$ at $z = 0.15$. The

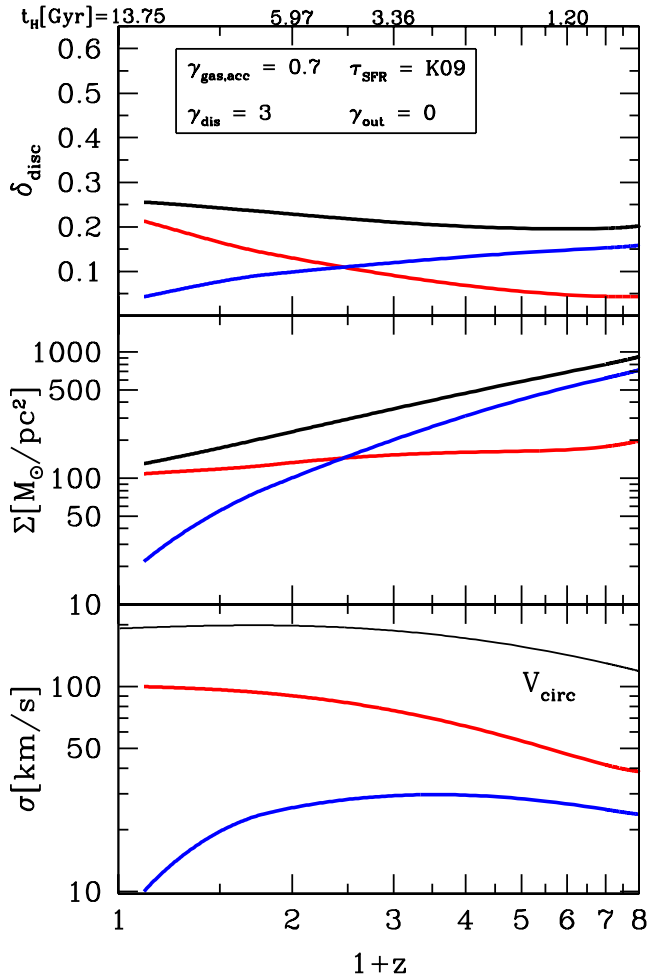


Figure 5. Evolution of the fiducial two-component model (Table 2). Panels and curves are as in Fig. 2. Shown are the quantities for the gas (blue), the stars (red), and their sum (black). The disc stabilizes at $z_{\text{stab}} = 0.15$.

evolution of σ_{gas} in the two-component fiducial model is similar to the evolution in the corresponding one-component gas model, except for the drop at $z \leq 1$. At $z = 2$, $\sigma_{\text{star}}/\sigma_{\text{gas}} \simeq 2.6$. Second, the total disc fraction within R_{disc} is rather constant in time, evolving in a quasi steady state as in the one-component gas model, at a comparable level of $0.2 - 0.25$, i.e., $B/D \simeq 2 - 1.4$, but here slowly rising instead of declining. The constancy of the bulge to disc ratio indicates that the massive bulge is not the main reason for the stabilization. Third, the stellar surface density in the fiducial model is almost constant throughout the disc evolution, contrary to its gradual decline in the one-component stellar model.

Figure 6 shows the evolution of the components of Q_{2c} , eq. (25), for the fiducial model. It shows the values of $Q = TQ$ for the gas and for the stars, with $T \simeq 1.5$ under the assumption of isotropy adopted here, and the value of W . We see that Q_{gas} is always smaller than Q_{stars} . This is because σ_{gas} is significantly smaller than σ_{stars} , and especially so when the surface density is dominated by the stars. For a similar reason W evolves to well below unity. As a result, Q_{gas} is dominant in determining Q_{2c} (eq. (25), top line), namely the instability is driven by the gas even after the disc has become stellar dominated.

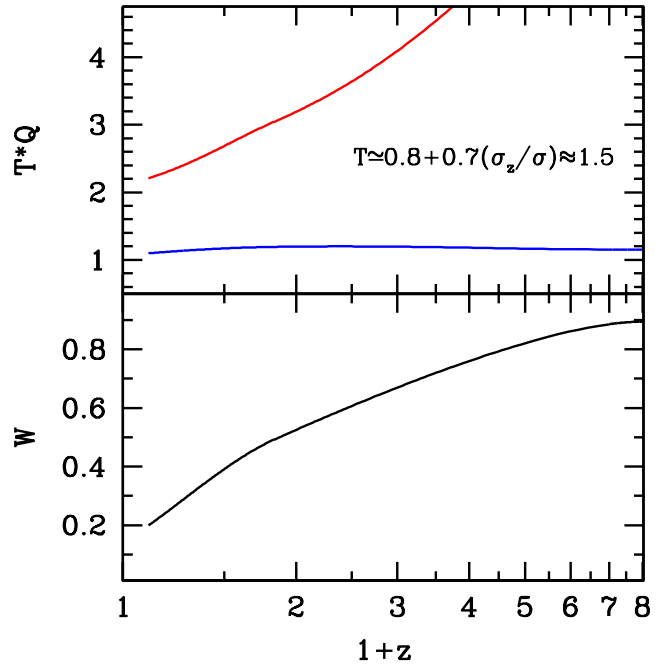


Figure 6. Evolution of the instability parameters in the fiducial two-component model. *Top:* The Q parameters, eq. (25), for gas (blue) and for stars (red). *Bottom:* The weighting function W , eq. (26). With a lower value of Q , the gas is the main driver of instability at all times.

4 VARIATIONS ABOUT THE FIDUCIAL MODEL

We now explore the effects of varying the model parameters that govern the turbulence dissipation rate (§4.1), the fraction of the baryonic cosmological input that joins the disc as gas (§4.2), the star formation rate (§4.3), and the outflow rate (§4.4). Table 2 displays the values of the parameters used in the different models.

4.1 Gas Dissipation

The energy considerations that lie at the basis of our model imply that the mass inflow rate within the disc is determined by the gas turbulence dissipation rate (eq. [3] and [21]) and that in turn the inflow down the potential gradient is the source of energy that adjusts the velocity dispersions of gas and stars at the level that guarantees $Q_{2c} = 1$. In Fig. 7, we test the effect of varying the dissipation parameter γ_{dis} (eq. (23)) between the extreme values 1 and 10, bracketing the fiducial value $\gamma_{\text{dis}} = 3$, while keeping the other model parameters at their fiducial values.

We notice first that the dissipation rate has only a minor impact on the qualitative behavior, and in particular on the time of stabilization, which shifts from $z_{\text{stab}} \approx 0.1$ to $z_{\text{stab}} \approx 0.3$ when γ_{dis} is varied from 10 to 1, corresponding to a shift from a slow to a fast inflow rate. A higher dissipation rate is responsible for a slightly earlier stabilization. The reason for the small effect is that, by construction, the ratio $\Sigma_{\text{gas}}/\Sigma_{\text{star}}$ is not very sensitive to the inflow rate, that is driven by the dissipation rate, and this ratio is in fact slightly higher for faster dissipation. The transition to star dominance varies from $z \simeq 1.3$ to 1.6 when γ_{dis} is varied from 10 to 1. Note that the surface densities of the two components are correlated not only because of the shared inflow and the resultant depletion of the two components of the disc, but also because according to the SFR prescription Σ_{star} is growing in proportion to Σ_{gas} . On the other hand, the value of γ_{dis} has a non-negligible

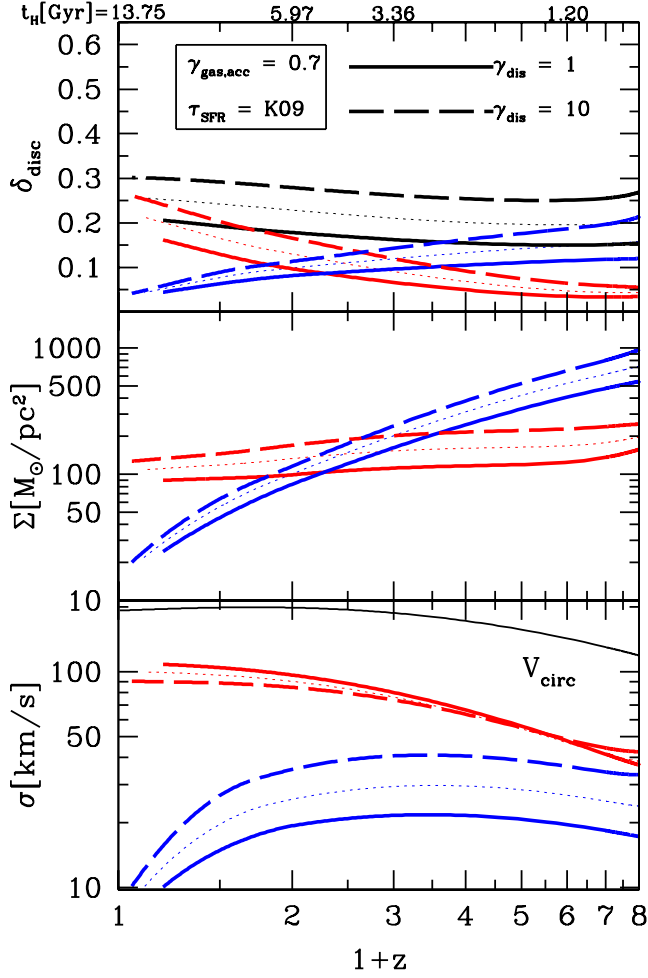


Figure 7. The effects of varying γ_{dis} (eq. (23)) in the range 1 – 10 on the evolution of the two-component model. Panels and curves are as in Fig. 5. Dotted curves refer to the fiducial model of Fig. 5 for comparison. The stabilization epoch is only weakly affected, but the gas dispersion velocity is significantly lower when the dissipation rate is higher.

effect on the value of σ_{gas} prior to its drop at $z \leq 1$, which is $\simeq 40 \text{ km s}^{-1}$ and $\simeq 20 \text{ km s}^{-1}$ for $\gamma_{\text{dis}} = 10$ and 1, respectively. The corresponding values of $V_{\text{circ}}/\sigma_{\text{gas}}$ at $z = 2$ are 4.2 and 7.4 for $\gamma_{\text{dis}} = 10 - 1$. While the drop of σ_{gas} may start a bit later for $\gamma_{\text{dis}} = 10$, the fact that it starts from a higher value makes it reach 10 km s^{-1} at a slightly later time.

We also see, in the top panel, that a higher dissipation rate, inducing a higher disc depletion rate, makes the total disc fraction smaller, from $\delta_{\text{disc}} \sim 0.25 - 0.3$ to $\sim 0.15 - 0.2$ when γ_{dis} is varied from 10 to 1. These correspond to $B/D \gtrsim 1$ and 2 respectively.

4.2 Effective Accretion onto the disc

Here, we explore the effect varying γ_{acc} (eq. (14)), the fraction of the average cosmological accretion rate that joins the disc as gas, using the extreme values $\gamma_{\text{acc}} = 0.4$ and 1 about the fiducial value of 0.7. Fig. 8 displays the results, showing that the stabilization time shifts from $z_{\text{stab}} \simeq 0$ to 0.4 when γ_{acc} varies from 1 to 0.4.

Higher values of γ_{acc} correspond to higher surface densities of the two components, because of the SFR dependence on Σ_{gas} . This dictates higher values of σ for the two components in order to maintain $Q_{2c} = 1$. Both $\sigma_{\text{star}}/\sigma_{\text{gas}}$ and $\Sigma_{\text{star}}/\Sigma_{\text{gas}}$ are rather

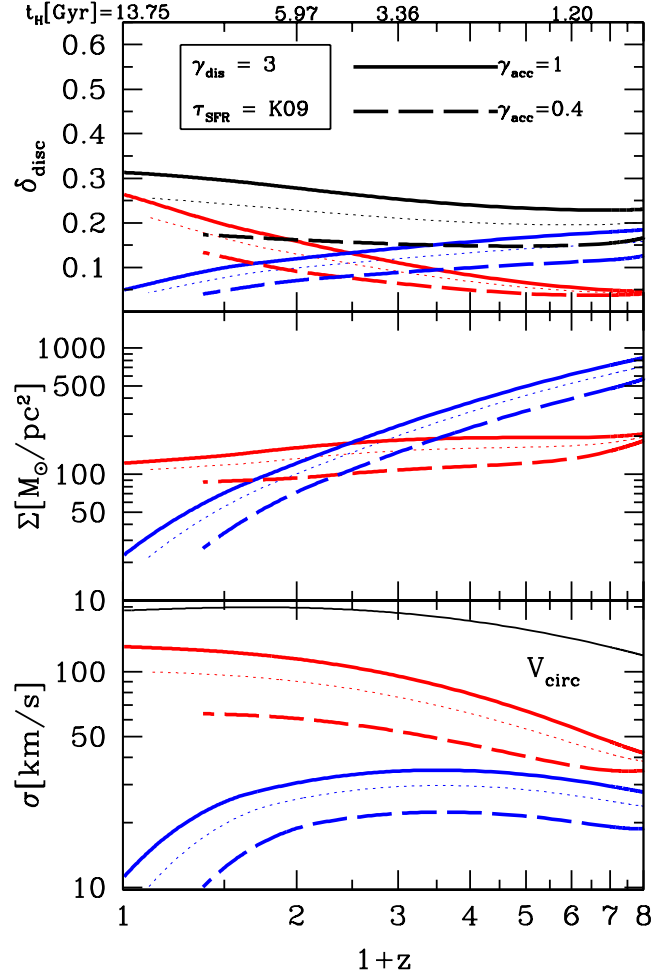


Figure 8. The effects of varying γ_{acc} (eq. (14)) in the range 0.4 – 1 on the evolution of the two-component model. Panels and curves are as in Fig. 5 and Fig. 7. The stabilization epoch is only weakly affected, but the gas dispersion velocity is lower when the accretion onto the disc is lower.

insensitive to γ_{acc} , and so are, in particular, the time of turning star dominated and when σ_{gas} starts dropping at $z \sim 1$. The case of higher γ_{acc} reaches 10 km s^{-1} later because it has to drop from a higher value at earlier times, 35 km s^{-1} for $\gamma_{\text{acc}} = 1$ compared to 20 km s^{-1} in the case of $\gamma_{\text{acc}} = 0.4$.

Note also in the top panel that a higher γ_{acc} corresponds to a higher disc fraction, varying from $\delta_{\text{disc}} \sim 0.17$ to 0.3 when γ_{acc} is varied from 0.4 to 1.

4.3 Star Formation

We next study the effect of varying the star formation efficiency per free-fall time, ϵ_{sfr} (eq. (15)), in comparison with our fiducial star-formation law of K09 eq. (16). Fig 9 shows the results for the cases with $\epsilon_{\text{sfr}} = 0.01$ and 0.05.

In order to help us interpret these results, we compare in Fig. 10 the star formation laws, in terms of Σ_{SFR} as a function of Σ_{gas} , for the three models studied here. We see that prior to $z \simeq 3$, the Σ_{SFR} in the $\epsilon_{\text{sfr}} = 0.01$ model is indeed slightly higher than in the K09 model, and it becomes lower after this time. On the other hand, the $\epsilon_{\text{sfr}} = 0.05$ model has a significantly higher Σ_{SFR} than

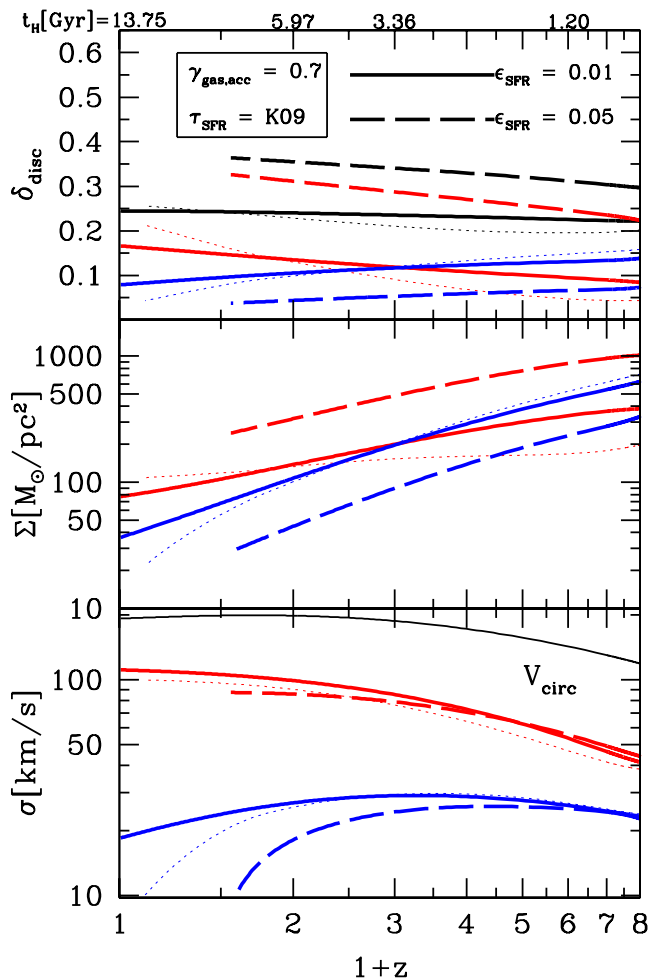


Figure 9. The effects of varying ϵ_{sfr} (eq. (15)) in the range 0.01 – 0.05 on the evolution of the two-component model. Panels and curves are as in Fig. 5 and Fig. 7. The stabilization epoch is rather sensitive to the SFR. The case of very high SFR is unique in the sense that it is always stellar dominated, and still, it maintains instability at high redshifts, to be stabilized only at late times.

the two other models at all times. We will see that this has an impact on the evolution of the instability.

The model with $\epsilon_{\text{sfr}} = 0.01$ remains unstable all the way to $z = 0$ with an almost constant disc fraction in a steady state at $\delta_{\text{disc}} \simeq 0.25$, namely $B/D \simeq 1.4$, not too different from the one-component model (§ 3.1 and DSC09). The reason is that the low SFR at late times allows the disc to never become strongly star dominated — it maintains $\Sigma_{\text{stars}}/\Sigma_{\text{gas}} < 2$ over a long period of time, from $z \sim 2$ to 0. This eliminates the factor that serves as the main driver for stabilization in the fiducial case. On the other hand, at very high redshift, Σ_{star} is higher than in the fiducial case. This is because in the high Σ_{gas} regime the SFR with a constant ϵ_{sfr} is higher than with the K09 law (see Fig. 10).

The case with very efficient SFR, $\epsilon_{\text{sfr}} = 0.05$, behaves very differently from all other models. While it stabilizes at $z \simeq 0.6$, somewhat earlier than the fiducial model, the very efficient SFR makes this disc strongly star dominated at all times, with $\Sigma_{\text{star}}/\Sigma_{\text{gas}} \simeq 2.8$ already at $z = 7$, growing to ~ 10 at later times. Despite the stellar dominance, the disc is unstable till after $z \sim 1$. The low gas fraction involves low dissipation and therefore slow inflow rate in the disc, making the disc fraction grow to above

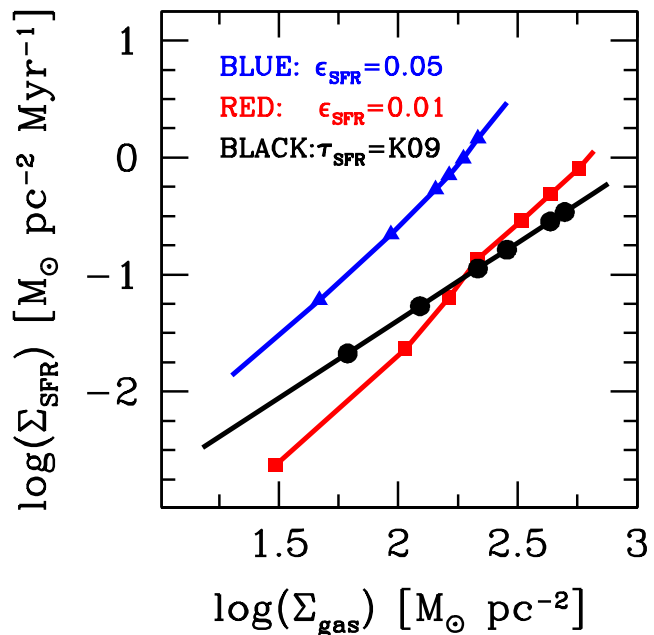


Figure 10. The SFR surface density as a function of gas surface density for different SFR prescriptions: the fiducial K09 prescription (black line, eq. (16)), and the two cases shown in Fig. 9, with $\epsilon_{\text{sfr}} = 0.01$ (red line) and 0.05 (blue line). The points refer from right to left to $z = 6, 5, 4, 3, 2, 1$, with the $\epsilon_{\text{sfr}} = 0.01$ extending to $z = 0$. The SFR in the $\epsilon_{\text{sfr}} = 0.01$ case is higher than the fiducial model at early times, and lower at low redshifts.

$\delta_{\text{disc}} = 0.35$. The reason for the rather decline of σ_{gas} starting at $z \sim 2$ towards stabilization at $z \simeq 0.6$ is subtle, as no other quantity involved shows an abrupt change near that time. One thing that does change though is the rate of decline of Σ_{gas} , which at $z \sim 2$ becomes steeper than that of $\Omega \propto (1+z)^{3/2}$. When this happens, Q_{2c} can be maintained at unity only if σ_{gas} declines, and this decline is enhanced because Σ_{gas} is low.

4.4 Outflows due to Stellar Feedback

Figure 11 shows the effects of strong and very strong outflows via $\gamma_{\text{out}} = 1$ and 3 (eq. (17)). We see that the stabilization epoch shifts from $z_{\text{stab}} \simeq 0.15$ when outflows are ignored to $z_{\text{stab}} \simeq 0.5$ and 1 for $\gamma_{\text{out}} = 1$ and 3, respectively. This means that strong outflows could be the strongest driver towards early stabilization among the physical properties explored so far. The gas removal from the disc due to strong outflows causes a steep decline in Σ_{gas} , making it drop below $100 M_{\odot} \text{pc}^{-2}$ already prior to $z \simeq 1.5$ for $\gamma_{\text{out}} = 3$. This translates via $Q_{2c} = 1$ to a low gas velocity dispersion, dropping below 20 km s^{-1} already at $z \simeq 2.5$, from which the way to stabilization at 10 km s^{-1} is rather short. The disc fraction in the extreme outflow model becomes rather low, $\delta_{\text{disc}} \simeq 0.1$, namely a bulge-dominated system.

With an outflow rate comparable to the SFR, $\gamma_{\text{out}} = 1$, these effects are less drastic. While stabilization occurs at $z_{\text{stab}} \approx 0.5$, the disc fraction is rather constant at about 0.2, and the disc at z_{stab} has $\Sigma_{\text{stars}}/\Sigma_{\text{gas}} \approx 4$ and $\sigma_{\text{stars}}/\sigma_{\text{gas}} \approx 10$, all not that different from the fiducial model in which outflows were ignored.

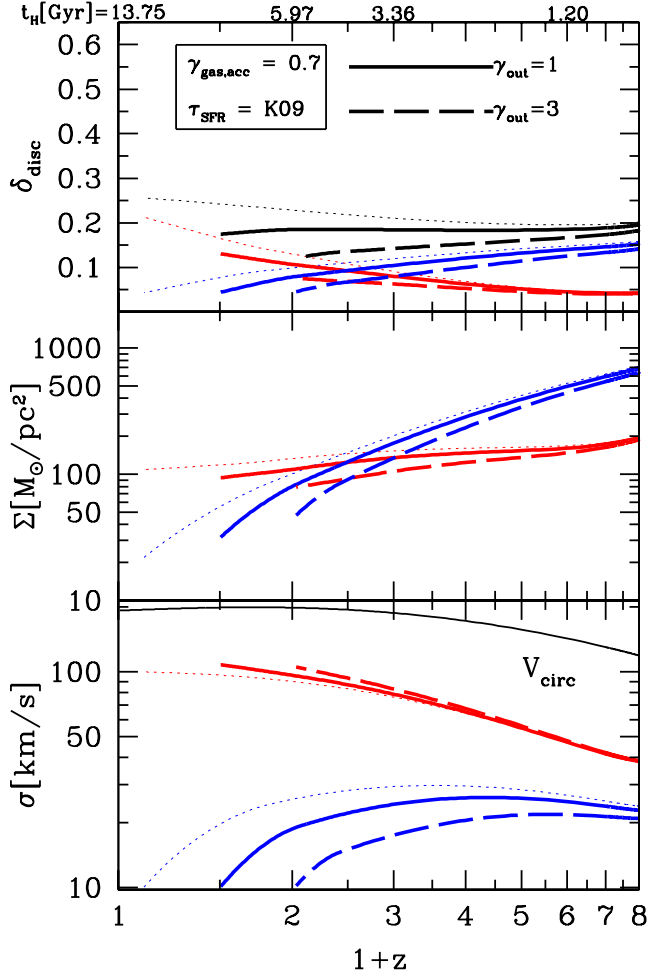


Figure 11. The effects of varying γ_{out} (eq. (17)) in the range 0 – 3 on the evolution of the two-component model. Panels and curves are as in Fig. 5 and Fig. 7. Stronger outflows induce earlier stabilization, but still limited to $z_{\text{stab}} \sim 1$.

4.5 A Case of Extreme Stabilization

In order to explore the robustness of the instability at high redshift, we present here a case in which the parameters are pushed to extreme limits within the sensible range, in an attempt to obtain early stabilization. This model has a very low fraction of gas accretion into the disc ($\gamma_{\text{gas,acc}} = 0.4$), a high dissipation rate ($\gamma_{\text{dis}} = 1$), a high outflow rate ($\gamma_{\text{out}} = 3$), and the K09 SFR law. Figure 12 demonstrates that even in such an extreme case the disc remains unstable until $z \approx 2$. At the time of stabilization, the surface density is not yet star dominated, but the low accretion rate and the strong outflows lead to a low total surface density, of $\Sigma \simeq 100 M_{\odot} \text{pc}^{-2}$ already by $z \simeq 2$. The disc fraction is low and roughly constant at $\delta \simeq 0.1$, i.e., the system is bulge dominated with $B/D \approx 5$. Thus, the disc stabilization in this case could be interpreted as driven by “morphological quenching” due the massive bulge (Martig et al. 2009) rather than by the transition to a star-dominated disc. We conclude that stabilization before $z \sim 2$ is very unlikely — it may be achieved only with more extreme outflows or in galaxies where the accretion is severely suppressed compared to the cosmological average.

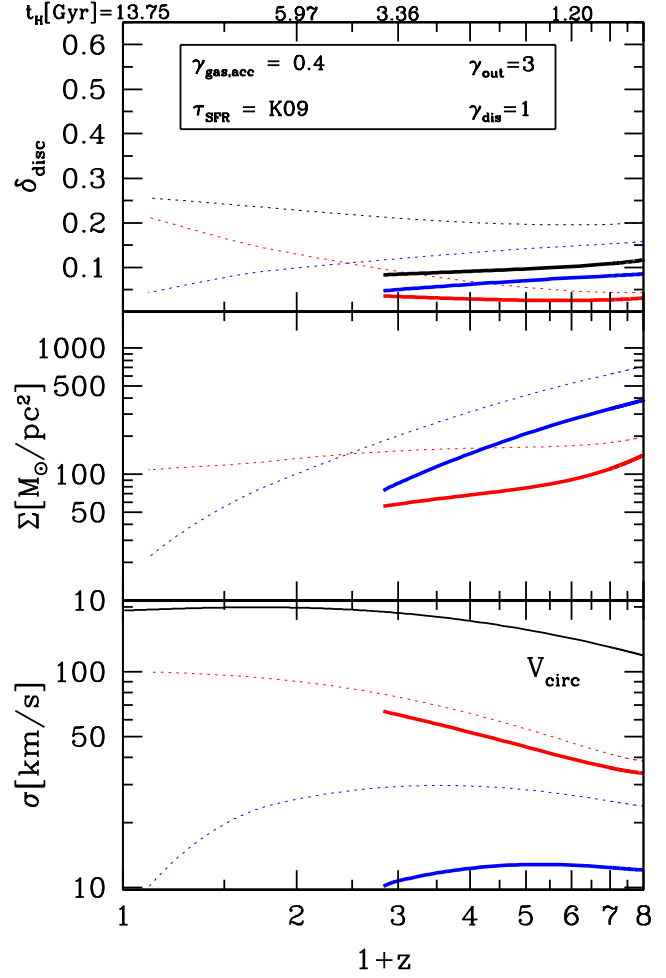


Figure 12. The effects of pushing the model parameters to extreme values favorable of early stabilization on the evolution of the two-component model. Panels and curves are as in Fig. 5 and Fig. 7. Even in this case, stabilization occurs only after $z = 2$.

5 DISCUSSION AND CONCLUSIONS

We have studied the cosmological evolution of gravitationally unstable galactic discs. To this aim, we have developed an analytic model that evolves in time the properties of a galactic disc as a sequence of quasi steady-state configurations under the assumption of self-regulated two-component gravitational disc instability. The disc is assumed to be fed by fresh gas at a constant fraction of the average cosmological accretion rate. The gravitational instability is associated with mass inflow within the disc towards a central bulge. In the disc, gas continuously turns into stars according to a given star formation law. This typically leads to a characteristic pattern of evolution from a gas-dominated disc at high redshifts to a star-dominated disc at low redshifts, which is the main driver of instability at high redshifts and the main reason for stabilization after $z \sim 1$.

The model is based on three key constraints, namely mass and energy conservation and self-regulated instability. Mass conservation accounts for cosmological accretion onto the disc, mass inflow within the disc into a central bulge, conversion of gas into stars, and gas outflows. Energy conservation imposes that the gravitational energy gain due to the mass inflow down the potential gradient is driving velocity dispersion in the disc gas and stars, com-

pensating for the dissipation of the gas turbulence on a dynamical timescale. The imposed self-regulated two-component instability then provides a connection between the velocity dispersions of gas and stars, which allows us to solve the set of equations and propagate the system in time.

While confirming that a single component disc, of gas or stars, is likely to maintain the instability in a steady state till $z = 0$ (DSC09), we find here that a two-component disc, where gas continuously turns into stars, tends to (a) be unstable at $z > 1$ and (b) stabilize at $z \sim 0 - 1$. The instability at high redshift is typically driven by the high surface density of gas and “cold” stars, which is due to the high density of the universe and the high cosmological accretion rate. The stability at low redshift is typically driven by the stellar dominance, which results from the declining cosmological accretion rate, the decline of Σ because of the cosmological expansion, the continuous conversion of gas to stars, the outflows of gas, and the effects of inflows in the disc on disc depletion and bulge growth. The low gas surface density and its fraction in the disc forces the gas to a low velocity dispersion in order to balance the high stellar velocity dispersion and keep $Q_{2c} \sim 1$.

We study the impact of varying the assumed dissipation rate, fraction of gas accretion onto the disc, star formation law, and outflow rate. When the model parameters vary within a sensible range, the epoch of stabilization tend to change only in a limited range, typically $0.1 < z < 0.6$. The inclusion of strong outflows plays a somewhat more significant role, and it may stabilize the disc as early as $z \sim 1$ if the mass removal rate is three times the SFR. An extreme model, in which the parameters are all pushed to their most favorable values for early stabilization, is capable of shifting the stabilization to an earlier epoch, but only to $z \sim 2$. Prior to $z \sim 2$, it is difficult to avoid violent disc instability.

In a companion paper (Genel, Dekel & Cacciato 2011), we explore the alternative possibility that the disc turbulence is driven by the cosmological in-streaming in a non-self-regulated manner (as in DCS09). We find that also in this case the discs tend to evolve from instability to stability, and that σ/V_{circ} could be in the ballpark of the observed values at $z \sim 2$, with no need to appeal to feedback effects. However, in this case σ/V_{circ} is predicted to be independent of the actual value of the accretion rate, thus not reproducing the observed decline with time. When we do impose self-regulation at $Q \sim 1$, and introduce a duty cycle for the instability, we find a better agreement with the observational trends.

The current analysis is simplified in several ways that justify a few cautionary notes. First, the baryonic accretion is assumed to be at the average cosmological rate, while one expects significant variations in the accretion rate along the history of every galaxy and between different galaxies as a function of their environment. Since the accretion rate is the main driver of disc instability and the associated phenomena, these variations may have important effects on the evolution. The evolution of instability under realistic accretion histories will be addressed in a follow-up paper.

Second, in order to solve the set of equations, we had to make assumptions concerning the stellar inflow rate in the disc compared to the gas inflow rate, and especially how the gravitational energy gain by the inflow is distributed between stirring up turbulence in the gas and raising the velocity dispersion of the stars. Our assumptions boils down to assuming that (a) the mass inflow rate per unit mass, or the drift velocity, is the same for gas and stars, and (b) that the energy deposited per unit mass in the disc is the same for gas and stars. The participation of stars in the inflow within the disc is obvious from the fact that they dominate the giant clumps that are known from analytic estimates (DSC09 and references therein) and

simulations (Ceverino et al. 2011 and references therein) to migrate inward on an orbital timescale as a result of torques, inter-clump interactions, and dynamical friction. However, the validity of the assumptions adopted here for the exact behavior of the stars compared to the gas is still uncertain. We note, for example, that Forbes et al. (in preparation), in a study of a similar problem, are adopting a different assumption concerning the stellar migration rate (M. Krumholz and J. Forbes, private communication). The inflow rate in the two disc components, the migration of clumps compared to the inflow of disc mass outside the clumps, and the evolution of velocity dispersion in the two components in the context of gravitational instability are all being studied in detail using high-resolution cosmological simulations (Cacciato et al. in preparation).

Third, we focused here on massive galaxies, comparable in mass to the Milky Way and to the observed big clumpy discs at $z \sim 2$ (Genzel et al. 2006; 2008; Elmegreen & Elmegreen 2005). However, one should be aware of the possibility that the evolution of instability may be different in less massive galaxies. On one hand, at a given redshift, less massive galaxies tend to have a similar Ω but a lower total surface density, which would require lower velocity dispersions for maintaining $Q_{2c} \sim 1$, thus leading to earlier stabilization. On the other hand, if the less massive galaxies are more gas rich, as observed, perhaps due to different effects of star formation and feedback, then stabilization is expected later in less massive galaxies. There are indications for such a “downsizing” in instability in observations (Elmegreen & Elmegreen 2005) and in simulations (Bournaud et al. 2011). The mass dependence will be addressed in an upcoming paper.

Despite these limitations, our analysis indicates that phases of violent disc instability are a solid prediction at $z > 1$, and that the typical discs are likely to stabilize prior to the present epoch, mostly due to the growing dominance of “hot” stars at late times. The predictions of our analytic model are to be compared to those from high-resolution hydro-cosmological simulations.

ACKNOWLEDGMENTS

We acknowledge stimulating discussions with Frederic Bournaud, Andi Burkert, Daniel Ceverino, John Forbes and Mark Krumholz. This work has been supported by the ISF through grant 6/08, by GIF through grant G-1052-104.7/2009, by a DIP grant, and by an NSF grant AST-1010033 at UCSC. MC has been supported at HU by a Minerva fellowship (Max-Planck Gesellschaft). MC acknowledges the hospitality of the Dublin Institute for Advanced Studies and, together with AD, that of the Astronomy Department at UCSC.

REFERENCES

- Agertz, O., Lake, G., Teyssier, R., Moore, B., Mayer, L., & Romeo, A. B. 2008, MNRAS, 1373
- Birnboim, Y., & Dekel, A. 2003, MNRAS, 345, 349
- Bouché N., Murphy, M. T., Péroux, C., Csabai, I., Wild, V. 2006, MNRAS, 371, 495
- Bouché N., Murphy, M. T., Péroux, C., Davies, R., Eisenhauer, F., Förster Schreiber, N. M., Tacconi, L. 2007, ApJ, 669, 5
- Bouché N., et al., 2010, ApJ, 718, 1001
- Bournaud, F., Elmegreen, B. G., & Elmegreen, D. M. 2007, ApJ, 670, 237
- Bournaud, F. et al. 2008, A&A, 486, 741
- Bournaud, F. et al. 2011, arXiv:1107.1483
- Bullock, J. S., Dekel, A., Kolatt, T. S., Kravtsov, A. V., Klypin, A. A., Porciani, C., & Primack, J. R. 2001a, ApJ, 555, 240

- Bryan, G. L. & Norman, M. L., 1998, *ApJ*, 495, 80
Ceverino, D., Dekel, A., & Bournaud, F. 2010, *MNRAS*, 404, 2151
Daddi, E., et al. 2004, *ApJ*, 617, 746
Danovich, M., Dekel, A. 2011, arXiv:1110.0000
Davè, R., Finlator, K., Oppenheimer, B. D. 2011, arXiv:1108.0426
Dekel, A., & Birnboim, Y. 2006, *MNRAS*, 368, 2
Dekel, A., & Birnboim, 2008, *MNRAS*, 383, 119
Dekel, A. et al. 2009, *Nature*, 457, 451,
Dekel, A., Sari, R., Ceverino, D., 2009, *ApJ*, 703, 785
Elmegreen, B. G., & Elmegreen, D. M. 2005, *ApJ*, 627, 632
Fakhouri, O. Ma, C.-P., Boylan-Kolchin, M., 2010, *MNRAS*, 406, 2267
Fall, S. M. & Efstathiou, G., 1980, *MNRAS*, 193, 189
Gammie, C. F. 2001, *ApJ*, 553, 174
Genel, S. et al. 2008, *ApJ*, 688, 789
Genel, S. Dekel, A., Cacciato, M, 2011, arXiv:1111.0000
Genzel, R. et al. 2008, *ApJ*, 687, 59
Goldreich, P. & Lynden-Bell, D., 1965, *MNRAS*, 130, 97
Hopkins, P. F., Quataert, E., & Murray, N. 2011, arXiv:1101.4940
Immeli, A., Samland, M., Gerhard, O., Westera, P., 2004, *A&A*, 413, 547
Jog, C. J., & Solomon, P. M. 1984, *ApJ*, 276, 127
Joung, M. R., Mac Low, M.-M., & Bryan, G. L. 2009, *ApJ*, 704, 137
Kennicutt, R. C. 1989, *ApJ*, 344, 685
Kereš, D., Katz, N., Weinberg, D. H., & Davé, R. 2005, *MNRAS*, 363, 2
Khochfar, S. & Ostriker, J. P., 2008, *ApJ*, 680, 54
Komatsu, E., et al. 2011, *ApJS*, 192, 18
Krumholz, M. R., McKee, C. F., & Tumlinson, J. 2009, *ApJ*, 699, 850
Krumholz, M. R., & Burkert, A. 2010, *ApJ*, 724, 895
Krumholz, M. R. & Dekel, A., arXiv:1106.0301
Krumholz, M. R., Dekel, A., McKee, C. F., 2011, arXiv:1109.4150
Martig, M., Bournaud, F., Teyssier, R., & Dekel, A. 2009, *ApJ*, 707, 250
Martin, C. L. & Bouché, N. 2009, *ApJ*, 703, 1394
Mo, H. J., Mao, S., & White, S. D. M. 1998, *MNRAS*, 295, 319
Neistein, E., & Dekel, A. 2008, *MNRAS*, 383, 615
Neistein, E., van den Bosch, F. C., & Dekel, A. 2006, *MNRAS*, 372, 933
Noguchi, M., 1999, *ApJ*, 514, 77
Ocvirk, P., Pichon, C., Teyssier, R., 2008, *MNRAS*, 390, 1326
Ostriker, E. C., & Shetty, R. 2011, *ApJ*, 731, 41
Rafikov, R. R. 2001, *MNRAS*, 323, 445
Romeo, A. B. 1994, *A&A*, 286, 799
Romeo, A. B., & Wiegert, J., 2011, *MNRAS*, 416, 1191
Toomre, A. 1964, *ApJ*, 139, 1217
van den Bergh, S., Abraham, R. G., Ellis, R. S., Tanvir, N. R., Santiago,
B. X., & Glazebrook, K. G. 1996, *AJ*, 112, 359
van de Voort, F., Schaye, J., Booth, C. M., & Dalla Vecchia, C. 2011, *MNRAS*, 416, 805
Wang, B., & Silk, J. 1994, *ApJ*, 427, 759
Wechsler, R. H., Bullock, J. S., Primack, J. R., Kravtsov, A. V., & Dekel, A.
2002, *ApJ*, 568, 52